OE Optical Engineering

RESEARCH PAPER

First order solution generation and optimization of reflective dual-conjugate zoom systems

Doran S. Teverovsky,* Kendall A. Smith, and Julie L. Bentley
University of Rochester, Institute of Optics, Rochester New York, United States

ABSTRACT. Adaptive optics (AOs) ophthalmoscopy is a powerful technique for imaging retinas of living subjects at single-cell resolution. Traditional AO ophthalmoscopes use a fixed exit pupil diameter, which is matched to the ocular pupil of a subject. A more efficient ophthalmoscope would allow for a variable exit pupil size to match the variable ocular pupil size of a subject. One method to achieve this is an optical zoom system. To make a zoom system appropriate for use in adaptive optics ophthalmoscopy, it must be simultaneously well corrected for both the field conjugate and the pupil conjugate such that the aberration correction can be successfully applied. The system must also be made of reflective optics to minimize chromatic aberration and spurious back reflections propagating through the system. Both of these factors make for an zoom system that requires tools and methods to be developed to realize successful designs. We present here our work developing a first-order starting point generator, which creates valid first-order solutions that satisfy all the constraints of the system. We then show our techniques for modeling and optimizing the simultaneous conjugates of the system throughout the process of unobscuring the system. We find that to achieve the selected specifications that freeform optics must be used. These surfaces are critical for correcting the residual aberrations introduced in the unobscuring process.

 [DOI: 10.1117/1.OE.63.8.085103]

Keywords: adaptive optics; dual conjugate imaging; optical zoom systems; reflective optics; freeform optics

Paper 20240426G received Apr. 25, 2024; revised Jun. 25, 2024; accepted Jul. 17, 2024; published Aug. 10, 2024.

1 Introduction

Adaptive optics ophthalmoscopes (AOOs) are optical systems that are used to image retinas of living subjects at cellular-scale resolution.[1] They do this by employing dynamic aberration correction enabled by a closed-loop aberration control system, most commonly a Shack–Hartmann wavefront sensor and a deformable mirror (DM) both placed at conjugate planes to the ocular pupil. Many of these systems are made with reflective optics used off-axis to allow for a large bandwidth (400 to 1000 nm) with no chromatic aberration and minimal spurious back reflections that come from refractive surfaces used on axis.[2–5] AOOs have begun to see use in clinical settings, as their superior resolution could allow for early detection of common retinal diseases, such as age-related macular degeneration, glaucoma, and diabetic retinopathy, but also rarer diseases, such as Best disease, Stargardt's disease, and juvenile retinoschisis.[6–10] Until now, AOO systems have been designed with a fixed exit pupil (XP) size that matches a typical dilated ocular pupil size. This approach is satisfactory when all subjects can be dilated to a similar ocular pupil

*Address all correspondence to Doran S. Teverovsky, dtevero2@optics.rochester.edu

size but is ill-suited to subjects with smaller ocular pupil diameters, such as juveniles and older adults.[11,12] Current AOOs have small fields of view (FOV), typically ± 1.5 deg, which is set by the largest area that can be imaged while maintaining diffraction limited resolution through a fully dilated ocular pupil.[13,14] This diffraction limited area is called the isoplanatic patch. The size of the isoplanatic patch depends on many factors, but it critically has an inverse relationship with ocular pupil size.[15] When imaging through an ocular pupil smaller than the designed XP current, AOOs cannot increase the imaging FOV to take advantage of the larger isoplanatic patch. As such, there is a strong desire for a more flexible AOO design that can better serve a broader patient population. Such an instrument requires an AOO with a zoom optical system that can resize the XP of the system to closely match the ocular pupil size of a given subject while also reciprocally changing the FOV. By holding the product of the XP size and FOV to be constant, étendue is constant for the optical system. To make a system like this work, the two separate conjugate pairs (field and pupil) must be simultaneously well corrected.

2 First Order Solution Specifications and Generation

When designing a zoom system, it is common to begin with the first order constraints of the problem such that a valid first-order (VFO) solution can be generated and used as a starting point for the design. For a zoom system where both field and pupil conjugates must be controlled, there are more first-order constraints to satisfy for a VFO solution compared to conventional zoom lenses. The extra constraints also necessarily require more degrees of freedom to find a VFO starting point.

To handle the task of finding VFO solutions for a dual-conjugate zoom system, we developed a new solution generator using MATLAB that generates many VFO solutions with a Monte Carlo approach, similar to what has been shown in prior work.[16–18] This solution generator has great flexibility and can be used to generate starting points for many zoom system design problems, including refractive, catadioptric, or reflective zoom relays as presented here and camera lenses with specific EP/XP location requirements through zoom. For our specific design, the requirements that must be satisfied for the application are as follows.

- The system must be an afocal relay, with external EP and XP planes.
- The system must have a long relief between the EP/XP and the next optical surfaces. This is to allow for positioning the DM at the entrance pupil (EP) and eye relief for the subject located at the XP.
- The system must be all reflective and free of obscuration to minimize both chromatic aberration over the waveband and to maximize transmission efficiency.
- The system must nominally be simultaneously well corrected for both the field and pupil conjugates.
- To adapt to varying FOV and pupil size requirements, the system must be able to continuously vary between a large pupil/small field and a small pupil/large field configuration.
- The XP location and orientation must not change significantly while the pupil size is varied.

The specifications for our example design problem are shown in Table 1.

There is a simple heuristic for a functional zoom lens: the system needs to have at least as many variables that change through zoom as there are first order constraints that must be controlled through zoom. For a single conjugate zoom lens with a variable focal length, at least one lens must move. In such a lens, the image plane will move with focal length change. Two moving lenses are required to change focal length while the image plane remains fixed in space. An example of such a system is shown in Fig. 1(a), where it is imaging the EP onto the XP. We traditionally say that the first moving lens, the variator, introduces the appropriate focal length change, and the second moving lens, the compensator, brings the image back in focus on the desired location. For our afocal system, we must introduce a third moving lens. If the variator and compensator image the EP onto the XP at the appropriate size and location, the third moving lens ensures that the lens remains afocal in image space. We will also introduce fixed outer elements to allow enough variables to satisfy the remaining first order constraints. A schematic representation of a three moving lens system can be seen in Fig. 1(b).

Table 1 Critical specifications for the example problem presented in this work.

Specification	Target value		Notes
Wavelength	400 to 1000 nm		Reference wavelength of 587 nm
FOV (object space)	±1.5 deg		
EP diameter	14 mm		Size of an ALPAO DM97-15 mirror
EP clearance	≥100 mm		Space for DM body without clipping
Zoom ratio	2x		
	Large pupil zoom	Small pupil zoom	
FOV (image space)	±2.62 deg	±5.25 deg	
XP diameter	8 mm	4 mm	
XP clearance	≥150 mm		For eye relief
XP position variation through zoom	≤1 mm		Fixed XP position allows for zooming with no subject repositioning
Performance targets			
Average RMS wavefront error for field conjugate	≤λ/14		Maréchal criterion
Average RMS wavefront error for pupil conjugate	≤λ/2		Correlated with minimum required resolvable spots across the pupil for wavefront sensing and correction

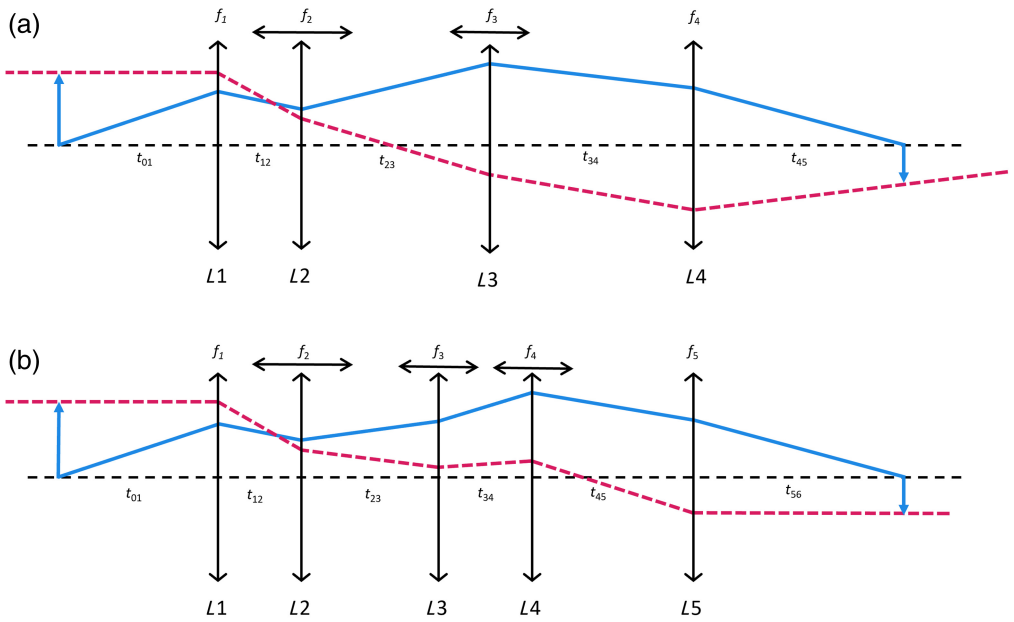

Fig. 1 (a) A four lens finite conjugate zoom system where the center two lenses are translated to create magnification change. This lens is being used to image a telecentric object, in blue, with the appropriate magnification and position through zoom. Note that the lens is telecentric only in object space and not image space as can be seen by the angle of the dashed red ray in image space. (b) A five lens, three moving lenses, and dual-conjugate zoom lens. The five lens system can achieve the required image space telecentricity while also maintaining magnification and image position. t_{nm} is the separation between surface n and m, and f_n is the focal length of lens n.

A typical method utilized for designing zoom lenses begins with solving a set of equations that calculates the necessary lens positions for a given set of component focal lengths and desired object/image distances. Using ABCD matrix optics formulations, the equations could be arranged as follows for a finite/finite zoom system with four lenses

$$\begin{bmatrix} 0 \\ M \end{bmatrix} = \mathbf{M_1} * \begin{bmatrix} 0 \\ 1 \end{bmatrix}, \tag{1}$$

$$\mathbf{M_1} = T(t_{45}) * R(f_4) \ldots R(f_1) * T(t_{01}), \tag{2}$$

$$T(t) = \begin{bmatrix} 1 & t \\ 0 & 1 \end{bmatrix}; \quad R(f) = \begin{bmatrix} 1 & 0 \\ -1/f & 1 \end{bmatrix}. \tag{3}$$

In practice, these equations can allow a lens designer to calculate lens separations for a given set of focal lengths, magnifications, and positions. This system of equations is simple enough to solve exactly, but the solutions will not always be real-valued or physically realizable for a given input set of focal lengths. Unfortunately, there is no way of knowing *a priori* what the best input component focal lengths and conjugate positions are. One common solution is to use a Monte Carlo search that can trial millions of input combinations and filter out invalid solutions like solutions with complex valued or negative lens separations.[16–19] Some designers will go a step further and perform initial ray traces and filter out lenses that are not ray traceable for the specified FOV and aperture size. The post-calculation filtering approach often has yields as low as 0.06% for generating lenses with valid component separations. Of those, typically approximately 10% will pass the initial ray trace filter. A consequence of this is that a lot of compute time is spent on lenses that are ultimately not useful to the designer.

For a dual-conjugate lens system of five lenses, the system of equations is as follows:

$$\begin{bmatrix} 0 \\ M \end{bmatrix} = \mathbf{M_2} * \begin{bmatrix} 0 \\ 1 \end{bmatrix}, \tag{4}$$

$$\begin{bmatrix} 1/M \\ 0 \end{bmatrix} = \mathbf{M_2} * \begin{bmatrix} 1 \\ 0 \end{bmatrix}, \tag{5}$$

$$\mathbf{M_2} = T(t_{56}) * R(f_5) \ldots R(f_1) * T(t_{01}). \tag{6}$$

The need to find a single matrix $\mathbf{M_2}$ that simultaneously solves Eqs. (4) and (5) through zoom raise the dimensionality of the total problem such that a generic algebraic expression covering all potential input values is impossible to derive without several simplifying assumptions. In practice, a computer aided solver must be utilized to calculate the necessary lens separations for a dual-conjugate zoom. By creating a solver that allows for the easy implementation of constraints onto output values, rather than filtering post-calculation, we can cull invalid solutions sooner in the calculation and limit the amount of time spent computing solutions that are not valid. We implemented our solver in MATLAB's symbolic math toolbox as it allows us to exactly solve the first order equations while also allowing us to introduce new direct constraints on output values that make generated solutions more likely to be valid. For example, we can reject all solutions with lens separations smaller than a given value, $t_{\min}$, at any given configuration. This parameter is free for the designer to tune as they please to restrict the solution space.

Unlike refractive lenses, which can get very close to each other with little issue, allowing mirrors to get too close to each other will result in a design that cannot be unobscured. If any separation calculated by the solver results in a mirror separation smaller than $t_{\min}$, the solution is discarded immediately, and no further data are calculated. We can also implement other constraints on the calculated solutions, such as total lens separation change through zoom, rate of separation change, or maximum separation. The outcome of this is proportionally fewer solutions entering the ray-trace stage of the solution generator, which is more computationally expensive per solution. Additionally, the solutions that did enter the ray-trace stage seemed to almost all pass the ray filter step, although that could be a result of the specific constraints we were using for our design problem and requires further study. The solutions generated when thickness-filtering was implemented were almost universally of high quality and were able to be optimized and unobscured readily without excessive ray trace errors or loss of the required

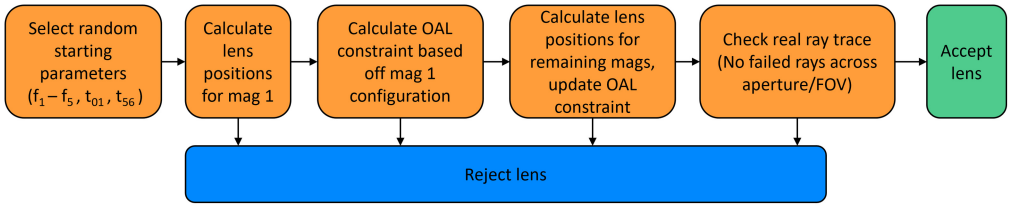

Fig. 2 A schematic representation of our Monte Carlo solution generator.

first order properties. Our solver also properly accounts for reflective and refractive surfaces when determining the overall length (OAL) constraint from EP to XP. Surfaces can be randomly assigned refractive or reflective per trial or assigned by the user. If every surface is refractive, the overall length constraint is simply the sum of all the air spaces. For a reflective system, the constraint must instead be the alternating sum of the air spaces to keep the XP fixed in space. A generalized length constraint for any system is

$$\mathrm{OAL} = \sum_{1}^{n} (-1)^{R(n)} * t_{(n-1,n)}, \tag{7}$$

where $R(n)$ counts the number of reflections before surface n, and $t_{(n-1,n)}$ is the air space from surface $n-1$ to n. Overall, our first order solution generation can be described with the flowchart shown in Fig. 2. The solution generator creates CODEV sequence files that can be directly loaded and manually inspected or can be further evaluated and optimized via the CODEV API. As is typical for zoom lenses, we discretize the continuous zoom motion into a finite number of configurations, five in this case, that represent a range of zoom positions from the lowest to the highest magnification.

3 Modeling the Pupil Conjugate

Before we can unobscure and optimize our lens, we must first determine how to model both the field and pupil conjugates simultaneously. The two basic approaches we considered were:

1. Model the field conjugate using configurations 1–5, one configuration for each of five different magnifications. While optimizing, control the pupil conjugate using real ray constraints that will enforce good pupil imaging and any other necessary properties.
2. Create a duplicate set of zoom configurations (6–10) that are twinned with their originators (1–5) and zoom system parameters such that the duplicate configurations model the pupil conjugate.

Method 1 requires half as many zoom configurations as method 2, but requires more constraints during optimization. Additionally, method 1 does not allow the designer easy access to quality metrics of the pupil conjugate and instead must reconfigure their lens whenever direct evaluation of metrics, such as wavefront error or RMS spot size, are needed in the pupil conjugate. While method 2 requires more configurations compared to method 1, it does allow for direct evaluation of critical metrics and removes any constraints from the optimizer related to the performance of the pupil conjugate from method 1. Instead, the default CODEV error function can be relied on to push both conjugates to perform well, and the relative importance of each conjugate can be tweaked by changing the weights in the optimizer of configurations 1–5 relative to 6–10.

In CODEV, a lens designer is allowed to zoom almost any parameters that describes their lens system, including system specification values such as field points, EP diameter, and object space telecentricity, so method 2 has a lot of promise for modeling our system. However, the designer cannot zoom the way that the field or the aperture is defined. If the system is defined using field angles and EP diameters for configurations 1–5, configurations 6–10 cannot be defined using object heights and numerical apertures. This poses a small issue as the most natural definition choice of aperture and field changes type between the field conjugate and the pupil conjugate. To address this, we modeled the field conjugate as a finite object with height very far

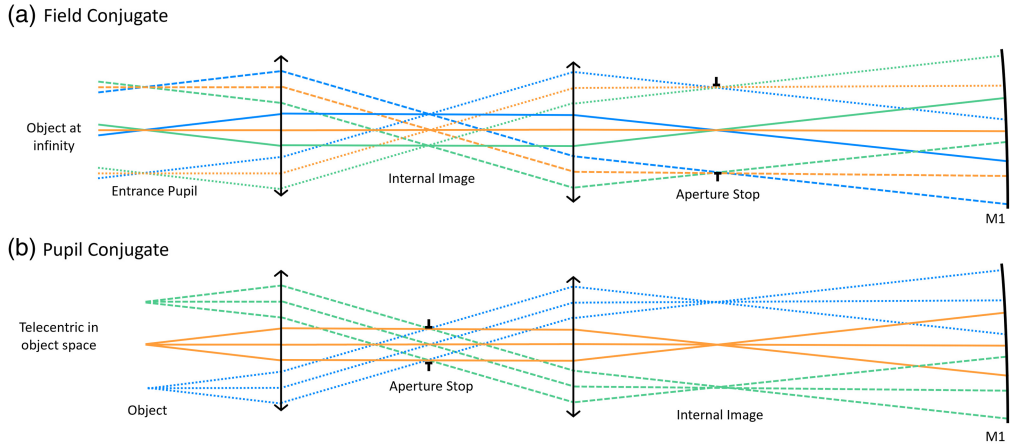

Fig. 3 (a) An afocal system modeled with an object at infinity. (b) The same system, modified to instead model the pupil conjugate. Ray color denotes field point in each respective conjugate, whereas the line type remains the same for rays that follow identical paths so the correspondence between the two systems can be seen.

away from the system, instead of as an object at infinity with field angles. Given the distance from the object to the EP, it is a simple trigonometry problem to determine the object heights and the numerical apertures that correspond to the natural field angles and EP diameters. If the entire process is done properly, a twinned pair of zooms should have marginal and chief rays that switch between configurations. Using pickups on all zoomed lens separations, the configurations stay exactly twinned. We also included a perfect thin lens relay before our lens system. The perfect lens relay allows access to a perfect internal image plane that is set as the aperture stop when modeling the pupil conjugate. A graphical comparison of the system in both the field and pupil conjugate is shown in Fig. 3. The full list of parameter changes for swapping from one conjugate to the other is shown in Table 2.

4 Unobscuring and Optimizing the Design

Unobscuring a reflective design is often an iterative process of slowly decreasing the overall obscuration by increasing lens decenters, tilts, or field/aperture offsets and re-optimizing the system. Ultimately for a reflective zoom system, the process is very similar but with some extra configurations to check for ray clipping and some additional constraints to enforce. We opted to utilize mirror tilts as our primary variable to unobscure the system as is commonly done in reflective ophthalmoscope design and freeform optical design. This stage of the design process is when the unobscured system tilting geometry is set. The system tilting geometry is largely determined by the tilt directions of the mirrors, which will change which side of the incoming beam the next surface will be placed on, but it can also be influenced by the magnitude of the tilt.

Table 2 A full list of system parameters that change when modeling the field and pupil conjugate and the values used for our system.

Parameter	Field conjugate	Pupil conjugate
Object distance	$1e^{10}$ mm	0 mm
Object NA	$7e^{-10}$	0.0262
Telecentric EP	No	Yes
Obj. height h_{max}	$1.31e^{8}$ mm	7.00 mm
Afocal image space	Yes	No
Stop surface	EP	Internal image

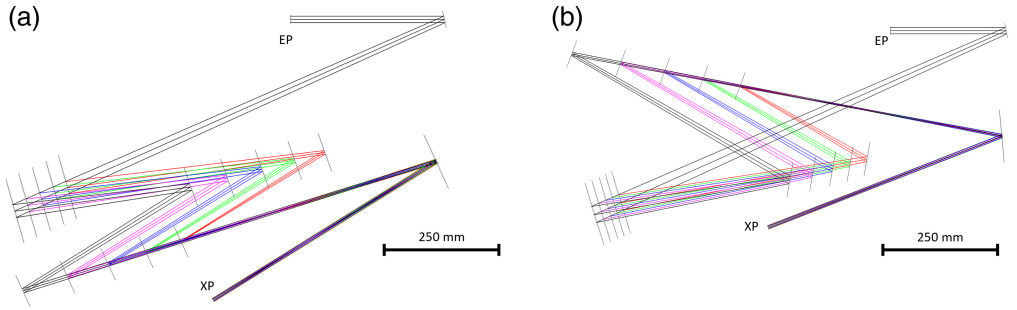

Fig. 4 Two systems derived from the same starting point with different geometries. (a) The alternating geometry has a gut ray that never intersects itself. (b) A design with a gut ray that crosses itself several times. Both lenses have similar overall performance. Ray fans are colored by configuration.

Different choices in tilting geometry have strong impacts on the final system quality after optimization for fixed optical designs.[20] The same is true for zoom system designs. For our particular zoom system, we must also ensure that our geometry choice allows for an easily accessible EP and XP and that no zoom motions overlap for two different mirrors. We anticipate that any physical prototype of this optical system would use translation stages to position the mirrors, which would make overlapping zoom motions difficult to realize. In Fig. 4, we show two intermediate designs derived from the same first-order starting point. These designs are similar to other reflective spherical systems seen in the past.[21] The alternating geometry automatically controls overlapping zoom motions and accessible pupils. System geometry also has a large impact on total system volume, and the alternating geometry does tend to require a larger overall system volume. The more compact geometry is more challenging to work with. There are many more potential ray clips to check/control, which can lead to more constraints in the optimizer that drive the design away from best optical performance. While this geometry does allow for a smaller system volume than the alternating geometry, we are operating in a regime where we are not strongly constrained by system volume or weight. As such, we opted to use only the alternating geometry for the remaining designs.

One impactful constraint at this stage of the design process is the fixed XP position. The XP position is constrained by ensuring that all the chief rays emanating from the field configurations come to a common point at the center of the XP. While normally only a single chief ray from the edge of the field is needed to determine pupil locations, chief rays in both x and y are needed to maintain the XP position for our tilted system. A consequence of this constraint is that the absolute position of mirror 5 does not change through zoom. For a system with no pupil control, the position of mirror 5 will also move through zoom unless directly constrained. However, constraining mirror 5 to be fixed through zoom is also sufficient to force convergence to a solution with a fixed XP position through zoom. In Fig. 5, we show a pair of designs demonstrating this. Each design is derived from the same starting point with the same bending geometry. Both designs have surface tilts, surface figure, and surface positions as variables and have the same constraints present during optimization, with the exception of pupil overlap control.

The design shown in Fig. 5(a) has only three moving mirrors, even though there is no direct constraint on keeping M5 fixed through zoom. This is because of our choice of moving mirrors and zoomed variables. With M2/3/4 moving in the YZ plane, but not changing surface normal orientation through zoom, the XP will be fixed in space through zoom if and only if M5 is also fixed in space through zoom. This relationship does not necessarily hold for a different choice of moving mirrors and/or zoomed variable. In such cases, an additional constraint would be necessary to keep M5 fixed through zoom along with the XP.

Figure 5(b)'s design has an XP that moves over 100 mm through zoom. This extra degree of freedom leads to a system with overall better wavefront performance compared to the system in Fig. 5(a), particularly for the field conjugate. The magnitude of performance improvement varies based on starting point and the optimization pathway, but a 10x improvement for the field conjugate and a 2x improvement for the pupil conjugate is typical. These improvement factors are in reference to the RMS wavefront error averaged over the whole FOV for each individual

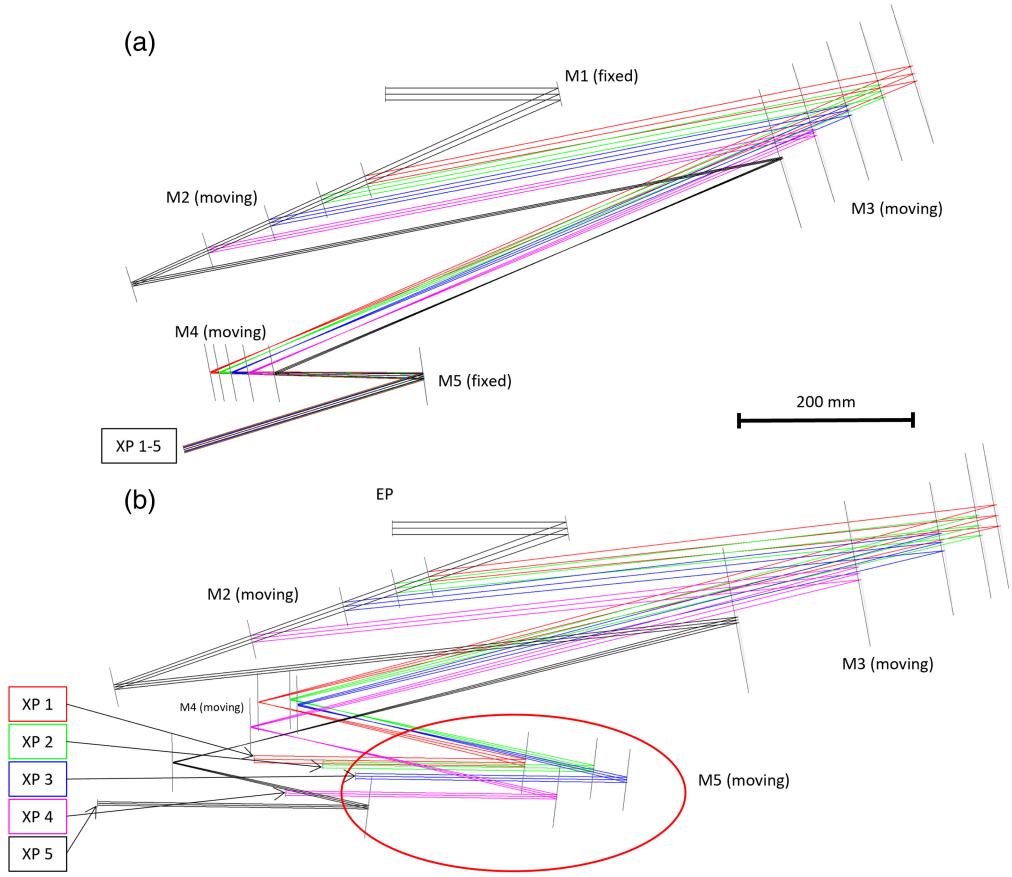

Fig. 5 Two designs that show how surface overlap constraints affect the optical system. (a) A design with overlap control on the XP surface. Even though M5 is not directly constrained, it does not move through zoom as can be seen by the perfectly overlapping M5 in panel A. (b) A design with no surface overlap control at all, which results in a moving XP and moving M5 through zoom. Ray fans are colored by configuration.

configuration. It should be noted that some starting points will converge poorly if the pupils are not constrained to overlap early in the design process. This is due to the extra degrees of freedom allowing the optimizer to find local minima in the optimization space earlier in the design process. These minima can be shallower than the local minima found with a surface overlap constraint.

We found that spherical mirrors were insufficient for achieving the wavefront performance required over the entire zoom and étendue while maintaining a fixed XP position. We utilized full-field display aberration maps and the principles of nodal aberration theory to evaluate what aberrations and/or constraints were limiting the system.[22,23] After optimizing, most of the starting points for our system were limited by the pupil conjugate RMS wavefront error and the overlapping XP constraint. The RMS wavefront error of the pupil conjugate in these systems was primarily limited by third order astigmatism. Among the best tested solutions, astigmatism in the pupil conjugate was significantly reduced, but still limiting along with third order coma in the pupil conjugate.

By switching from spherical to toroidal mirrors, we were able to correct much of the residual pupil conjugate astigmatism and improve our systems by 13.3x on average. At this point, most of the systems regardless of choice in starting point end up at similar performance levels as measured by average RMS wavefront error through zoom. We believe this is because the system has a relatively low étendue. With a small étendue, the system is driven by the first order, geometric constraints, and third order aberrations, rather than fifth and higher order aberrations.

Freeform optical surfaces can be used to further improve the system. To date, there has not been much work published on freeform optical zoom systems, nor on the effects of freeform

optics on aberrations of the pupil conjugates.[24] However, we can still leverage the same principle of nodal aberration theory to inform us of the effects of freeform surfaces in our optical system. A well-known result from nodal aberration theory is that an arbitrary freeform surface will have a different effect on the aberrations measured across the image plane depending on how far away from the aperture stop the surface is.[23] A surface at a pupil plane will impart a field-constant base effect. As the surface is moved away from a pupil plane, there is usually also a field-varying effect that scales with distance from the pupil in addition to the base effect. When the freeform surface is moved to an image plane, the surface contributes only field varying global phase across the image. We can extend this example to a simultaneous dual-conjugate design by realizing that the pupil and field are duals of each other. We can interchange object and EP all the same aberration results will still hold as we move a freeform surface along the optical system. Ultimately, this means that a given freeform surface will impart the same residual types of aberrations, albeit in differing magnitudes, to both the field and the pupil conjugates.

As an example, we consider third order coma, which is modeled in Fringe Zernike polynomials by Z7/8. We can correct field-constant third-order coma in the pupil conjugate by allowing Fringe Zernike Z7/8 departures onto some mirrors and optimizing. Any Z7/8 added to the system to correct the pupil conjugate coma will also add some field-constant third-order coma to the field conjugate. But, if before adding Z7/8 the field conjugate is already well-corrected third-order coma, then the addition of Z7/8 will degrade performance. Optimization might be able to recover performance, but it is not a guarantee. The one exception is if a freeform can be placed at or near an internal image, where it will have a smaller effect on the field performance and can be used to disproportionately impact the pupil conjugate. The disadvantage of this is that it requires a mirror to be near an internal image plane, where any imperfections or debris that stick to the surface will be re-imaged and superimposed onto the field conjugate image. We can summarize as follows: a system that can benefit most from freeform optics should have similar aberration residuals for both conjugates so that both can benefit from the same freeform polynomial surface departures.

Figure 6 shows one optimized freeform optical system that is near our target specifications. The impact of freeform varies strongly with number of Zernike terms included. We opted to use Fringe Zernike polynomials up to and including Z20 that respected the planar symmetry of the system. Higher-order rotationally symmetric terms Z25, Z36, and Z37 were also used. Despace and power degeneracy as described by Takaki[25] were controlled using constraints during optimization.

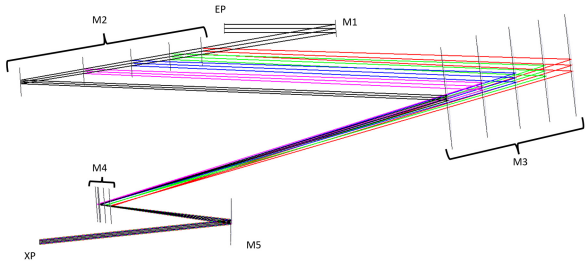

	Base Radius	Airspace	Tilt
EP	---	200 mm	0°
M1	1924.24 mm	239 – 589 mm	7°
M2	- 837.52 mm	667 – 772 mm	-9°
M3	1093.98 mm	897 – 626 mm	11.63°
M4	- 776.48 mm	242 – 220 mm	-13°
M5	613.24 mm	369 mm	12°
XP	---	---	-1°

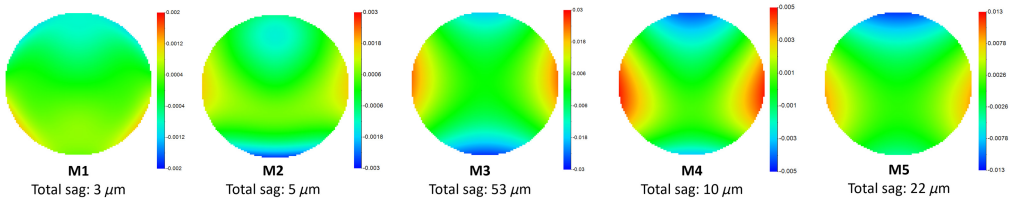

Fig. 6 One example freeform system derived from a starting point created via our solution generator. A basic surface prescription is shown, where the value for zoomed airspaces at position 1 and 5 is given. Extended surface data can be found in the data repository. The surface departure plots are drawn over the used surface apertures fit to a best fit sphere, and the sag values are shown in millimeters. Total sag for each surface is detailed below each plot.

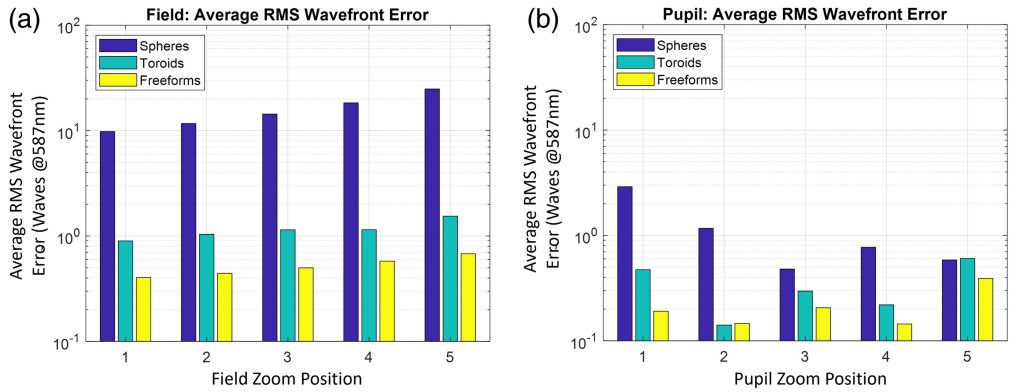

Fig. 7 A comparison of the wavefront performance of the design shown in Fig. 6 with two other designs derived from the same starting point with less complex surface definitions. Bars represent waves of error measured at 587.56 nm.

Figure 7 shows the effect of surface complexity on system performance by comparing the freeform system from Fig. 6 with a similar spherical design and a toroidal design. Each system began from the same inline starting point and was optimized with the specified surface type from the start of the manual unobscuring process. The systems were unobscured by progressively constraining minimum surface tilts until the system was fully unobscured for each zoom configuration. The field performance was uniformly improved by on average 13.3x moving from sphere to toroid and by 2.22x moving from toroid to freeform. The pupil was less uniformly improved, mostly due to the difficulty in correcting the highest mag configuration, configuration 5. Moving from sphere to toroid yields a 4.10x improvements and toroid to freeform yields a 1.59x improvement.

5 Discussion

There remain several challenges to be addressed before a system such as the ones presented in this work can be practically assembled. First, a method to move the optics accurately over relatively long distances needs to be selected. Linear stages can be purchased that have total travels of over 300 mm while maintaining 5 μm positional repeatability. Preliminary tolerance results show that our systems are not sensitive to 5 μm of axial error, but a more rigorous analysis would be necessary before we can say with certainty that 5 μm would be sufficient. A single stage of this type would be sufficient for mirror 2 and mirror 4. Unfortunately, mirror 3 would need two stages, stacked orthogonally, or otherwise some sort of mechanical system to change a linear or rotational motion into a curvilinear motion. If mirror 3's total translation was kept smaller, it might be practical to use a hexapod mounting scheme instead, which would be able to handle both axes of motion. In the designs presented here, the mirrors do not tilt through zoom. However, it is conceivable that such a degree of freedom might be useful for future designs. A single linear actuator could be used to achieve this as long as the mirror is well centered to the rotational center of the mount so that it is a purely rotational motion. The long term stability of any proposed system would need to be investigated before a final determination can be made.

The current designs also do not meet specification when including the highest magnification configuration, which has a magnification of approximately 4x. When this configuration is removed for some designs, the remaining configurations improve upon re-optimization to be at the performance target specified in Table 1. Alternatively, a smaller DM could be used in the EP, which would bring the most extreme magnification of the system closer to unity. For example, an 8 mm DM would have a most extreme magnification of only 2x if all other specifications remained the same. In this work, we also did not model the DM that sits at the EP of the system. This mirror can be used as an additional degree of freedom that changes through zoom, which can be very powerful for cleaning up the field performance. Care needs to be taken when doing so to ensure that the DM is not using more sag than can be afforded, as it also needs to correct the subject aberrations.

6 Conclusion

We successfully created a first-order Monte Carlo solution generator for simultaneous dual-conjugate zoom systems. Using this tool, we generated over 400 VFO starting points, of which >99% of the solutions were ray-traceable. The direct-output filtering method we employed in our Monte Carlo successfully limited the solution space and reduced the total computation time spent on failed solutions. We can also generate compensated reflective, refractive, and catadioptric zoom systems by dynamically updating the constraint in the Monte Carlo solver to account for the types of optical surfaces appropriately. Most of the solutions generated (>80% of tested solutions) were readily unobscured while maintaining first order properties. Freeform optics show significant promise for correcting the aberrations in both conjugates that are introduced via the unobscuration process when tilting mirrors.

Disclosures

The authors have no competing interests to disclose.

Code and Data Availability

MATLAB code for the generation of VFO solutions can be found at https://github.com/dorant43/Reflective-Zooms.

Acknowledgments

We would like to thank Professor Alfredo Dubra for providing the details motivating the specifications for the selected application. We would also like to thank Mathworks and Synopsys for providing the MATLAB and CODEV licenses used in this work.

References

1. D. R. Williams et al., "Evolution of adaptive optics retinal imaging [Invited]," *Biomed. Opt. Express* **14**, 1307–1338 (2023).
2. A. Roorda et al., "Adaptive optics scanning laser ophthalmoscopy," *Opt. Express* **10**, 405–412 (2002).
3. A. Gómez-Vieyra et al., "First-order design of off-axis reflective ophthalmic adaptive optics systems using afocal telescopes," *Opt. Express* **17**, 18906–18919 (2009).
4. A. Dubra and Y. Sulai, "Reflective afocal broadband adaptive optics scanning ophthalmoscope," *Biomed. Opt. Express* **2**, 1757–1768 (2011).
5. S. Mozaffari et al., "Wide-vergence, multi-spectral adaptive optics scanning laser ophthalmoscope with diffraction-limited illumination and collection," *Biomed. Opt. Express* **11**, 1617–1632 (2020).
6. Y. Zhang et al., "Imaging of age-related macular degeneration by adaptive optics scanning laser ophthalmoscopy in eyes with aged lenses or intraocular lenses," *Transl. Vis. Sci. Technol.* **9**, 41 (2020).
7. Z. M. Dong et al., "Adaptive optics optical coherence tomography in glaucoma," *Progr. Retinal Eye Res.* **57**, 76 (2017).
8. I.-E. Cristescu et al., "High-resolution imaging of diabetic retinopathy lesions using an adaptive optics retinal camera," *Rom. J. Ophthalmol.* **63**(1), 29–34 (2019).
9. M. Georgiou et al., "Adaptive optics imaging of inherited retinal diseases," *Br. J. Ophthalmol.* **102**, 1028–1035 (2018).
10. H. Song et al., "High-resolution adaptive optics in vivo autofluorescence imaging in Stargardt disease," *JAMA Ophthalmol.* **137**, 603–609 (2019).
11. A. Bogdan, J. J. Weiter, and J. Tang, "The relationship of aging on pharmacologic pupil dilation and pupillary marginal tears," *Investig. Ophthalmol. Visual Sci.* **50**, 4835 (2009).
12. M. Guillon et al., "The effects of age, refractive status, and luminance on pupil size," *Optometry Vis. Sci.* **93**, 1093–1100 (2016).
13. G. Han et al., "Isoplanatic patch of the human eye for arbitrary wavelengths," *Opt. Commun.* **410**, 811–816 (2018).
14. D. Fried, "Anisoplanatism in adaptive optics," *JOSA* **72**, 52–61 (1982).
15. P. Bedggood et al., "Characteristics of the human isoplanatic patch and implications for adaptive optics retinal imaging," *J. Biomed. Opt.* **13**, 024008 (2008).
16. A. J. Yee et al., "New tools for finding first-order zoom lens solutions and the analysis of zoom lenses during the design process," *Proc. SPIE* **9580**, 958006 (2015).
17. M. C. Bruggeman and J. L. Bentley, "Determining optimal first-order focal lengths of zoom lenses through Monte Carlo simulations," *Proc. SPIE* **11106**, 1110605 (2019).

18. D. H. Lippman, D. S. Teverovsky, and J. L. Bentley, "Monte Carlo first-order design method for anamorphic cinema zoom lenses," *Opt. Eng.* **60**, 051203 (2021).
19. M. E. Jungwirth, D. V. Wick, and E. L. Dereniak, "Theory and tradespace analysis of a reflective axial adaptive optical zoom system," *Opt. Eng.* **51**, 083001 (2012).
20. A. Bauer, E. M. Schiesser, and J. P. Rolland, "Starting geometry creation and design method for freeform optics," *Nat. Commun.* **9**, 1756 (2018).
21. J. M. Howard and B. D. Stone, "Imaging with three spherical mirrors," *Appl. Opt.* **39**, 3216–3231 (2000).
22. J. R. Rogers, "Techniques and tools for obtaining symmetrical performance from tilted-component systems," *Opt. Eng.* **39**, 1776–1787 (2000).
23. K. Fuerschbach, J. P. Rolland, and K. P. Thompson, "Theory of aberration fields for general optical systems with freeform surfaces," *Opt. Express* **22**, 26585–26606 (2014).
24. A. Bauer et al., "Multiconfiguration afocal freeform telescopes," *Opt. Express* **32**, 6154–6167 (2024).
25. N. Takaki, A. Bauer, and J. P. Rolland, "Degeneracy in freeform surfaces described with orthogonal polynomials," *Appl. Opt.* **57**, 10348–10354 (2018).

Doran S. Teverovsky is an optics PhD candidate at the University of Rochester studying adaptive optics ophthalmoscope design. He received his BS degree in optics from the University of Rochester in 2020. He is a member of SPIE.

Kendall A. Smith is an optics PhD student at the University of Rochester studying optical design. She received her BS degree in optical engineering from the University of Rochester in 2024. She is a member of SPIE.

Julie L. Bentley received her BS, MS, and PhD degrees in optics from The Institute of Optics at the University of Rochester. She is currently a professor of optics at the University of Rochester, an optical design consultant, and vice president of SPIE.